The Influence of Interfaces on Properties of Thin-Film Inorganic Structural Isomers Containing SnSe–$NbSe_2$ Subunits

Matti B. Alemayehu,* Matthias Falmbigl, Kim Ta, and David C. Johnson*

Department of Chemistry and Materials Science Institute, University of Oregon, Eugene, Oregon 97403, United States

ABSTRACT Inorganic isomers $([SnSe]_{1+\delta})_m(NbSe_2)_n([SnSe]_{1+\delta})_p(NbSe_2)_q$-$([SnSe]_{1+\delta})_r(NbSe_2)_s$ where m, n, p, q, r, and s are integers and $m + p + r = n + q + s = 4$ were prepared using the modulated elemental reactant technique. This series of all six possible isomers provides an opportunity to study the influence of interface density on properties while maintaining the same unit cell size and composition. As expected, all six compounds were observed to have the same atomic compositions and an almost constant c-axis lattice parameter of ≈4.90(5) nm, with a slight trend in the c-axis lattice parameter correlated with the different number of interfaces in the isomers: two, four and six. The structures of the constituents in the ab-plane were independent of one another, confirming the nonepitaxial relationship between them. The temperature dependent electrical resistivities revealed metallic behavior for all the six compounds. Surprisingly, the electrical resistivity at room temperature decreases with increasing number of interfaces. Hall measurements suggest this results from changes in carrier concentration, which increases with increasing thickness of the thickest SnSe block in the isomer. Carrier mobility scales with the thickness of the thickest $NbSe_2$ block due to increased interfacial scattering as the $NbSe_2$ blocks become thinner. The observed behavior suggests that the two constituents serve different purposes with respect to electrical transport. SnSe acts as a charge donor and $NbSe_2$ acts as the charge transport layer. This separation of function suggests that such heterostructures can be designed to optimize performance through choice of constituent, layer thickness, and layer sequence. A simplistic model, which predicts the properties of the complex isomers from a weighted sum of the properties of building blocks, was developed. A theoretical model is needed to predict the optimal compound for specific properties among the many potential compounds that can be prepared.

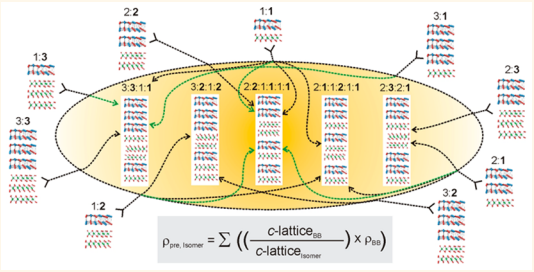

KEYWORDS: inorganic isomers · transport properties · charge transfer · interfaces · nanostructure

Over the past two decades, progress in nanotechnology had a great impact on research fields such as chemistry, materials science and physics.[1] For most nanotechnological applications, controlling interface structure and composition is critical for high performance and establishing a relationship between interfaces and device performance is also of fundamental interest. For example, considerable progress in improving thermoelectric materials has been achieved by overcoming trade-offs between bulk material properties, such as electrical resistivity, Seebeck coefficient and thermal conductivity.[2,3] The significant improvement in the figure of merit was accomplished by a reduction in phonon thermal conductivity due to increased phonon scattering due to grain size and nanoinclusions,[4] and there is also evidence for grain size induced changes in the density of states leading to enhanced power factors.[5] For nanostructured solar cell materials, the energy conversion efficiencies were significantly improved compared to bulk materials, mainly *via* controlled interface engineering.[6] The key for gaining a detailed knowledge of the mechanisms of enhancements in nanostructures is understanding the impact of structure and influence of interfaces on properties. Multilayer films with designed interfaces provide opportunities to gain this understanding and several studies on films with epitaxial interfaces have been reported. The strain that results from the lattice mismatch between

* Address correspondence to matti@uoregon.edu, davej@uoregon.edu.

Received for review February 12, 2015 and accepted April 8, 2015.

Published online April 08, 2015
10.1021/acsnano.5b01770

the films and the substrate causes a Jahn–Teller distortion, which significantly affects transport and magnetic properties.[7] Deconvoluting the effect of interfaces from that of strain due to epitaxial growth has been nearly impossible.[7]

Previously, it was demonstrated that multilayer films without an epitaxial relationship to the substrate or between constituents of the film could be synthesized *via* the modulated elemental reactants technique (MER).[8] The compounds formed have been called ferecrystals due to extensive turbostratic disorder between well-defined two-dimensional crystalline layers of the constituents.[9−11] The MER technique allows the formation of intergrowth compounds with a general formula of $([MX]_{1+\delta})_m(TX_2)_n$, where M = Sn, Pb, Bi, T = V, Nb, Ta, Mo, W, X = Se and/or Te, and δ is the structural misfit between the MX and TX_2 and $1 \leq m,n \leq 32$ are the number of the constituent layers. The ability to systematically vary the layering sequence and number of constituents in ferecrystals presents an opportunity to precisely control the structure and fine-tune physical properties at a subnanometer scale,[12] which was clearly demonstrated by the recent synthesis of the first inorganic structural isomers of $([PbSe]_{1.14})_m(NbSe_2)_n$.[13] For these isomeric compounds, different electrical resistivities dependent on the stacking sequence of the compound were observed.[13] The rotational disorder between constituents eliminates strain and the lattice mismatch between constituents results in nonepitaxial interfaces without strong directional bonding. The in-plane lattice parameters of the constituents are independent of one another. Previously, transport property measurements on different substrates demonstrated that the structure and nature of the substrate have a negligible influence on the properties of the thin film compounds.[14] The unique structural properties combined with their independence from substrate effects make ferecrystals ideal candidates for the investigation of interfacial effects on transport properties.

Here we report the synthesis and transport properties of the six inorganic isomers $([SnSe]_{1+\delta})_m(NbSe_2)_n$-$([SnSe]_{1+\delta})_p(NbSe_2)_q([SnSe]_{1+\delta})_r(NbSe_2)_s$ with $m + p + r = n + q + s = 4$ where m, n, p, q, r and s are integers. The six isomers, letting A = SnSe and B = $NbSe_2$ are $(A)_4(B)_4$, $(A)_3(B)_3(A)_1(B)_1$, $(A)_3(B)_2(A)_1(B)_2$, $(A)_2(B)_3(A)_2(B)_1$, $(A)_2(B)_1(A)_1(B)_2(A)_1(B)_1$ and $(A)_2(B)_2(A)_1(B)_1(A)_1(B)_1$. The short hand notation 4:**4**, 3:**3**:1:**1**, 3:**2**:1:**2**, 2:**3**:2:**1**, 2:**1**:1:**2**:1:**1**, and 2:**2**:1:**1**:1:**1** will be used in the remainder of this manuscript, where the number represents the consecutive structural units of each type, the normal and bold fonts represent the different structural units, and the order of the numbers denotes the structural units in the unit cell. Except for potential small changes in the misfit parameter due to structural changes with thickness, all these compounds have the same *c*-axis lattice parameter and composition. The 4:**4** compound has two interfaces per unit cell, while the 3:**3**:1:**1**, 3:**2**:1:**2** and 2:**3**:2:**1** compounds have four and the 2:**2**:1:**1**:1:**1**, and 2:**1**:1:**2**:1:**1** compounds have six. Taking advantage of the unique structural and substrate independence of ferecrystals, the influence of interfaces on the electrical transport properties of these six structural isomers was investigated. The electrical resistivity, carrier concentration and mobility are very similar for the six isomers, but change systematically with the thickness of the constituent layers. The properties cannot be described as a simple composite of the properties of the bulk constituents, as the data suggest that there is significant charge transfer between the constituents, which depends primarily on the thickness of the SnSe layers. The thickness of the individual $NbSe_2$ layers is the major factor controlling carrier mobility. The separation of the function of the constituent layers suggests that such heterostructures can be tailored through choice of constituent, layer thicknesses and layer sequences to tune particular properties and enhance performance.

RESULTS AND DISCUSSION

Synthesis and Structural Properties. To synthesize the targeted structural isomers, a sequential calibration procedure was performed to prepare precursors with nanoarchitectures that mimic the desired products.[15] Briefly, a series of Sn |Se and **Nb**|**Se** precursors were prepared by sequentially depositing elemental layers to determine the ratio of deposition times that correspond to the composition of the desired binary constituents, SnSe and $NbSe_2$. A sequence of Sn|Se|**Nb**|**Se** precursors was then deposited varying the amount of Sn|Se relative to the amount of **Nb**|**Se** to determine the ratio of the binary layers that produces the desired misfit ratio. Holding all of the elemental ratios constant, the overall thickness of a series of Sn|Se|**Nb**|**Se** precursors was then varied to determine the thickness that produced a pair of (100) planes of rock salt structured SnSe and a single Se–Nb–Se trilayer of dichalcogenide structured $NbSe_2$ after annealing. The six different inorganic isomers were synthesized by preparing sequences of these calibrated precursor layers that mimicked the layers in the targeted product, for example to form the 2:**2**:1:**1**:1:**1** compound, a Sn|Se|Sn|Se|**Nb**|**Se**|**Nb**|**Se**|Sn|Se|**Nb**|**Se**|Sn|Se|**Nb**|**Se** sequence was repeated until the desired film thickness was reached.

To self-assemble the final product, the precursors were annealed for 20 min at 400 °C.[12] After annealing, the compositions of all six compounds were measured using EPMA and were found to have the same atomic composition within error, as expected because the same number of layers of each constituent were deposited in the precursors. The specular 00*l* X-ray patterns of the annealed precursors are displayed in Figure 1, which indicates that highly oriented crystalline nanostructures were formed. All of the Bragg maxima can be indexed as

00*l* reflections and all six isomers have reflections at the same angles due to their similar *c*-axis lattice parameters (see Table 1). Each isomer has a distinct set of intensities for the reflections, however, because of the different stacking sequence of the layers, there is a slight increase in the *c*-axis lattice parameter with increasing number of interfaces. This results from the larger interlayer spacing between $NbSe_2$−SnSe compared to the sum of $NbSe_2$−$NbSe_2$ and SnSe−SnSe distances, but the differences are at the limit of the instrumental precision. Each additional interface between the two constituents results in a 0.1−0.2 nm increase in the *c*-axis lattice parameter.

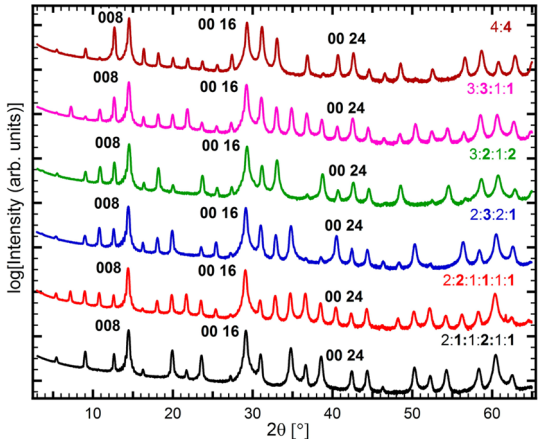

Figure 1. Specular 00*l* X-ray diffraction patterns with selected Bragg reflections indexed.

Grazing incidence in-plane X-ray diffraction measurements were conducted to determine the in-plane lattice dimensions of the constituent compounds. Typical for ferecrystals,[9,16] independent lattices were observed for each constituent (see Figure 2a) and the same diffraction patterns were obtained on silicon and fused silica substrates because no epitaxial relationship exists between the constituents or with the substrate. All the reflections could be indexed as (*hk*0) reflections. Similar to earlier reports, differences in the line widths of (*hh*0) and (*hk*0) reflections suggest the basal plane of the 4:**4** compound is rectangular rather than square.[17] The Bragg reflections of the SnSe for the remaining five isomers were indexed to a square basal plane. The *a*-axis lattice parameters for the SnSe constituent are within the reported range for misfit layer compounds and ferecrystals.[12,18] The $NbSe_2$ reflections could be indexed to hexagonal symmetry. The in-plane lattice parameter of the $NbSe_2$ ranges between those reported for the 2*H*- and 1*T*-bulk polytypes: 0.3449(1)−0.3460(1) and 0.353(1) nm, respectively.[15,20,21] Although the volume fraction of the constituents remains constant in all six isomers, the intensity ratio between the (220) SnSe peak and the (110) $NbSe_2$ peak continuously decreases as the layer thickness of the SnSe blocks decreases (see Figure 2b).

TABLE 1. Number of Interfaces between the Two Constituents, *c*-Lattice (For Two Sets of Isomers) and In-Plane Lattice Parameters, Area of SnSe and $NbSe_2$ and Misfit Parameter of All the Isomers from Set 1

isomer	number of interfaces	*c*-axis lattice parameter set 1 [nm]	*c*-axis lattice parameter set 2 [nm]	SnSe, *a*-axis lattice parameter [nm]	SnSe in-plane area, [nm^2]	$NbSe_2$ *a*-axis lattice parameter [nm]	$NbSe_2$ in-plane area [nm^2]	misfit δ
4:**4**	2	4.86(5)	4.87(3)	0.604(1)[a]	0.364[a]	0.3462(1)	0.104	0.14
3:**3**:1:**1**	4	4.88(1)	4.89(1)	0.601(1)	0.361	0.3462(1)	0.104	0.15
3:**2**:1:**2**	4	4.88(2)	4.88(2)	0.601(1)	0.361	0.3464(1)	0.104	0.15
2:**3**:2:**1**	4	4.89(5)	4.90(3)	0.600(1)	0.360	0.3464(4)	0.104	0.15
2:**2**:1:**1**:1:**1**	6	4.91(2)	4.90(2)	0.599(1)	0.359	0.3464(5)	0.104	0.16
2:**1**:1:**2**:1:**1**	6	4.90(3)	4.90(2)	0.599(1)	0.359	0.3461(2)	0.104	0.16

[a] Corresponds to a rectangular basal plane with *a*- and *b*-lattice parameters of 0.4296 and 0.4241 nm, respectively, with an area of 0.182 nm^2.

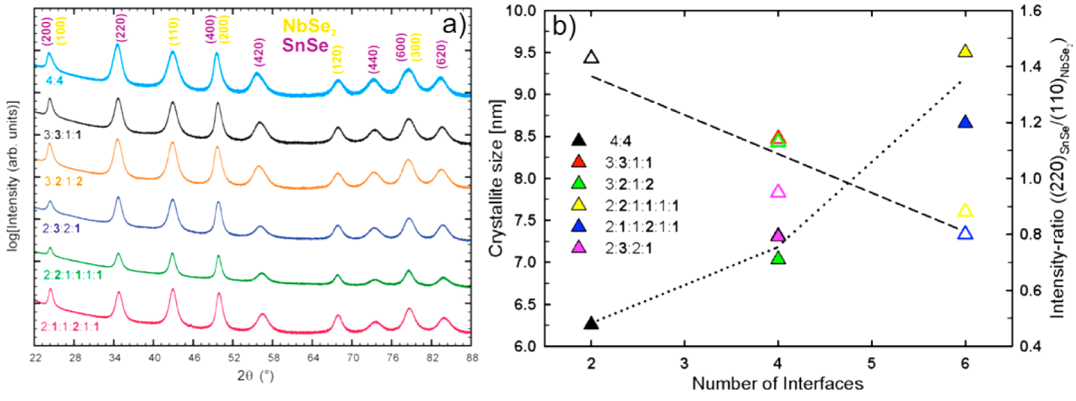

Figure 2. (a) Grazing incidence in-plane X-ray diffraction patterns of all the six $([SnSe]_{1+\delta})_m(NbSe_2)_n$ isomers. (b) Crystallite size of $NbSe_2$ (filled triangles) and intensity (open triangles) ratio of SnSe (220) to $NbSe_2$ (110) reflections as a function of interfaces. The dashed and dotted lines are guides to the eye.

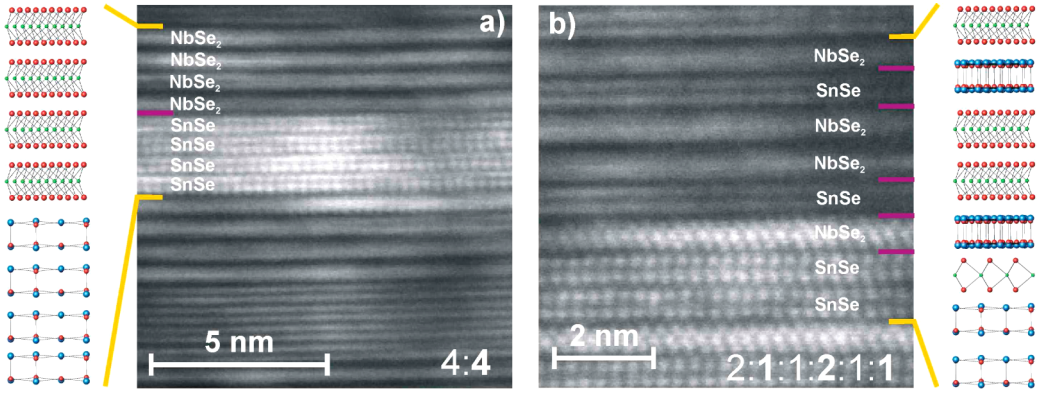

Figure 3. HAADF-STEM images of the 4:4 (a), and the 2:1:1:2:1:1 (b) isomers. The purple lines indicate interfaces between the two constituents. For both compounds, a structural schematic for one repeat unit is given (Larger area STEM images are provided in the Supporting Information in Figure S1).

In prior studies of SnSe−$NbSe_2$ ferecrystals, the SnSe forms a single domain between each $NbSe_2$ layer. This change in intensity might reflect smaller in-plane domain sizes as the block thickness decreases. The crystallite size of $NbSe_2$, obtained assuming the coherence length of the scattering is only due to crystallite size and using the Scherrer equation, also increases as the layer thickness of $NbSe_2$ decreases. Since it was shown earlier that the dichalcogenide layers template off one another, this templating will be reduced in isomers containing thinner $NbSe_2$ blocks leading to larger grain sizes.[22] An earlier report on $([SnSe]_{1.16})_1(NbSe_2)_n$[19] also reported smaller crystallite size with increasing thickness of the $NbSe_2$ constituent.

To further investigate the nature of the different interfaces, HAADF-STEM images were collected. Figure 3 shows representative HAADF-STEM images of two of the six isomers: 4:**4** and 2:**1**:1:**2**:1:**1**. Two and six interfaces can clearly be seen in the images. Figure 3a shows four double layers of SnSe and four layers of $NbSe_2$ with rotational disorder between subsequent layers, which is evident by the different crystal faces observed in different layers. Figure 3b highlights the structural unit of a 2:**1**:1:**2**:1:**1** compound, which also exhibits rotational disorder. In both cases, the crystallographic orientation within each SnSe block is the same. The STEM images show atomically abrupt and sharp interfaces at every interface. There is also significant in-plane rotational disorder between the constituents, as zone axes are only visible in some layers. These specific images were chosen as the zone axes enable the crystal structures of the layer to be directly observed.

Electrical Properties. The temperature dependent electrical resistivity of the isomers is shown in Figure 4. All six compounds exhibit metallic temperature dependence with a magnitude within a narrow range of (3.9−5.2) × 10^{-6} Ω·m at room temperature. The temperature dependence is similar in all compounds, decreasing linearly by about 1.6 × 10^{-6} Ω·m as temperature is decreased from room temperature to 50 K. Below 50 K, the resistivity is almost independent of

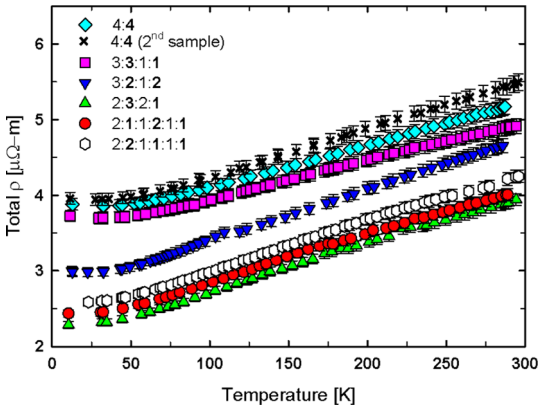

Figure 4. Temperature dependent electrical resistivity for all six isomers with an additional electrical resistivity data set for the 4:4 compound.

temperature. The very weak temperature dependence suggests a small electron−phonon coupling, reflecting the lack of 3D phonons due to the extensive rotational disorder as discussed previously in the literature.[14,23] The change in the structure of the isomers does not fundamentally change the nature of the conduction or the strength of the electron−phonon interaction. The resistivity does not systematically change with the number of interfaces. The three lowest resistivity curves are for isomers which all contain a layer with 2 bilayers of SnSe. The next highest are the two isomers that contain a layer with 3 bilayers of SnSe. The highest resistivity was found for the 4:**4** isomer. In general, the resistivity increases as the thickness of the thickest SnSe block in the isomer becomes thicker.

To get a deeper insight into the electronic transport properties, Hall measurements were conducted and the temperature dependent data for the six isomers are shown in Figure 5. Positive Hall coefficients were measured for all the six isomers, indicating that the majority carriers are holes as was found for bulk $NbSe_2$.[24] A common feature of the temperature dependent Hall coefficient for all isomers is a slight increase below 100 K indicating localization of carriers

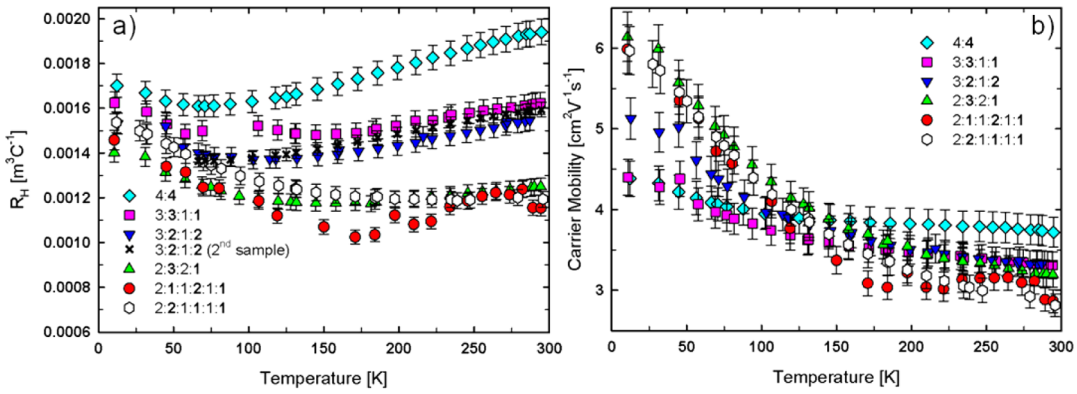

Figure 5. Temperature dependent Hall coefficients (a), and calculated Hall mobility (b) based on a single band approximation for all six isomers with an additional Hall coefficient data set for the 3:2:1:2 compound.

(see Figure 5a). In general, the Hall coefficient systematically decreases as the thickness of the thickest SnSe layer in the isomers decreases from 4 to 3 to 2. Using a single band approximation, carrier concentrations of all the isomers were calculated. The carrier concentration decreases from ≈5.2 × 10^{21} cm^{-3} for the isomers with two bilayers of SnSe to ≈3.9 × 10^{21} cm^{-3} for the isomers containing a block with three bilayers of SnSe to 3.3 × 10^{21} cm^{-3} for the 4:**4** isomer. These values cluster together much closer than the resistivity values, suggesting that the major effect of the SnSe nanoarchitecture is to control the number of carriers donated from SnSe to $NbSe_2$, with thicker blocks donating more electrons. Thicker blocks of SnSe were also observed to donate more charge in the compounds $([SnSe]_{1+\delta})_m(NbSe_2)_n$ when $m = n \leq 5$. This was attributed to the observed in-plane structural changes of SnSe as a function of thickness.[25] Systematic changes in interfacial disorder with increasing thickness of SnSe might also cause this effect.

The Hall mobility values vary only slightly, from 2.9 to 3.7 $cm^2\ V^{-1}\ s^{-1}$ at room temperature and the mobility increases as temperature is decreased for all of the isomers (see Figure 5b). The temperature dependence might be an artifact of assuming a single band model. Charge transport in misfit compounds is thought to be dominated by the dichalcogenide constituent.[26] Transport data collected on a series of $([SnSe]_{1+\delta})_m(NbSe_2)_1$ ferecrystals where m was varied from 1 to 10 showed that the mobility remained relatively constant, while the resistivity varied by a factor of 20 and the positive Hall coefficient varied by a factor of 50, strongly suggesting that the majority of the hole transport occurred through the metallic $NbSe_2$ layer.[12] We therefore expect that the mobility in the compounds studied here should trend with the nanoarchitecture of the $NbSe_2$ layer. The 4:**4** isomer has the highest mobility at room temperature. The two isomers with a block of 3 consecutive Se−Nb−Se trilayers and the isomer with two Se−Nb−Se trilayer thick layers all have about the same mobility at room temperature, ≈3.3 $cm^2\ V^{-1}\ s^{-1}$. The two isomers with two isolated Se−Nb−Se trilayers have the lowest mobility at room temperature, ≈2.9 $cm^2\ V^{-1}\ s^{-1}$. This observation indicates that the carrier mobility can be tuned by controlling the $NbSe_2$ thickness. The data presented here underscores the challenges in understanding the transport in these interleaved solids, where different constituents can serve different purposes. The transport data suggests that SnSe blocks donate charge to the $NbSe_2$ layers, which dominate the charge transport.

TABLE 2. Resistivity, Carrier Concentration, and Mobility of the Building Blocks from the Reports of the *m*:*n* Compounds

building blocks	resistivity [$\mu\Omega$-m]	carrier concentration [× $10^{21}cm^{-3}$]	mobility [$cm^2/(V\ s)$]	reference
(1,**1**)	3.95(8)	6.68(20)	2.60	14
(2,**2**)	4.69(9)	4.38(13)	3.04	28
(3,**3**)	4.71(9)	3.70(11)	3.60	25
(1,**2**)	3.81(8)	7.16(21)	2.28	20
(3,**2**)	5.25(10)	2.03(6)	5.86	28
(2,**1**)	6.44(13)	2.70(8)	3.60	12
(1,**3**)	4.12(8)	6.79(20)	2.24	20
(3,**1**)	7.86(16)	1.53(5)	5.19	12
(2,**3**)	5.25(11)	6.29(19)	2.10	-

In an attempt to create a model that could be used to predict properties of yet to be prepared compounds, we calculated the transport properties of the isomers from the sum of ($SnSe-NbSe_2$) building blocks. For example, the 3:**3**:1:**1** isomer can be broken into either 3:**3** + 1:**1** or 1:**3** + 3:**1** blocks. We calculated electrical resistivity, carrier concentration and the carrier mobility at room temperature for each building block from the measured values for the corresponding *m*:*n* compounds, listed in Table 2.[12,19,27] For the possible combinations for each isomer, we weighted the values for each building block based on its volume ratio within the isomer, essentially assuming they conduct independently in parallel. The calculated values for the isomers are listed together with the actually measured ones in Table 3. The model predicts the trend in carrier

TABLE 3. Actual and Calculated Resistivity, Carrier Concentration, and Mobility of the Isomer Compounds[a]

isomers	actual resistivity [$\mu\Omega$-m]	calculated resistivity [$\mu\Omega$-m]	actual carrier concentration [$\times 10^{21}$cm^{-3}]	calculated carrier concentration [$\times 10^{21}$cm^{-3}]	actual mobility [cm^2/(V s)]	calculated mobility [cm^2/(V s)]
4:**4**	5.17(10)	-	3.2(10)	-	3.8	-
	5.47(11)		3.1(9)		3.7	
3:**3**:1:1	4.91(10)	4.5[b]	3.8(11)	4.4[b]	3.3	3.1[b]
		5.9[b]		4.2[b]		2.5[b]
	4.99(10)		3.5(11)		3.6	
3:**2**:1:**2**	4.66(9)	4.7	4.0(12)	4.0	3.3	3.4
	4.85(10)		3.9(12)		3.3	
2:**3**:2:**1**	3.92(8)	5.3	5.0(15)	5.1	3.2	2.3
	4.05(8)		4.7(14)		3.3	
2:**2**:1:**1**:1:**1**	4.25(9)	4.3[b]	5.2(16)	5.5[b]	2.8	2.7[b]
		4.8[b]		5.4[b]		2.4[b]
	4.34(9)		5.0(15)		2.9	
2:**1**:1:**2**:1:**1**	4.03(8)	4.8	5.4(16)	5.4	2.9	2.4
	4.14(8)		5.7(17)		2.7	

[a] The calculated values use the data for the respective building blocks in Table 2. The actual resistivity and carrier concentration were obtained from measurements of two different sets of the isomers. [b] The electrical properties of these isomers were predicted by using different building blocks: for 3:**3**:1:**1**, the top row values were calculated from 3:**3** and 1:**1** building blocks and the bottom row values from 3:**1** and 1:**3**. For the 2:**2**:1:**1**:1:**1** isomer, the top row values were calculated from 2:**2** and 1:**1** building blocks, while the bottom row values were calculated from 1:**2**, 2:**1** and 1:**1**.

concentration reasonably well, with carrier concentration increasing from 3.2 $\times$ 10^{21} cm^{-3} to $\approx$4.2 $\times$ 10^{21} cm^{-3} to 5 $\times$ 10^{21} cm^{-3} as the thickness of the SnSe blocks decreases in size. The two different sums for the 3:**3**:1:**1** and 2:**2**:1:**1**:1:**1** isomers (see Table 3) provide similar values, indicating that charge transfer between the constituents depends mainly on the SnSe blocks, and not as much on the $NbSe_2$ layer and the different interfaces present. In general, the calculated carrier concentration agrees with the measured one, supporting the idea that charge transfer is governed by the thickness of the SnSe blocks rather than the types of interfaces. However, the model does a worse job of predicting the resistivity, which can be traced to the differences between the actual and the calculated mobility. The two different calculated mobility values for the 3:**3**:1:**1** isomer vary considerably, probably reflecting the limits of our ability to prepare samples with reproducible in-plane grain sizes and defect levels. The calculated mobility values generally trend downward as the thickness of the $NbSe_2$ layers decrease, which is in agreement with the measured values. While the model has limitations, a method to calculate the properties of yet to be made isomers *via* constituent parts would have considerable value, as over 20 000 compounds can be made containing ten or less SnSe and $NbSe_2$ layers in the unit cell. Theoretical calculations, grounded by accurately modeling the properties of a small set of compounds, that could predict which of the potential 20 000 compounds would have optimal properties for a particular application would be immensely valuable.

CONCLUSION

The six possible inorganic isomers, $([SnSe]_{1+\delta})_m(NbSe_2)_n([SnSe]_{1+\delta})_p(NbSe_2)_q([SnSe]_{1+\delta})_r(NbSe_2)_s$ where m, n, p, q, r and s are integers and $m + p + r = n + q + s = 4$ were synthesized *via* the modulated elemental reactant technique containing either two, four or six interfaces between the constituents per unit cell. The *c*-axis lattice parameters of all isomers were 4.90(5) nm and increase by 0.1 nm for each interface. The systematic change of intensity ratios of specular X-ray diffraction scans and HAADF-STEM images clearly demonstrate that six distinct compounds were synthesized. In-plane X-ray diffraction revealed independent lattice dimensions for the SnSe and the $NbSe_2$ constituent and only subtle differences between the six isomers. HAADF-STEM demonstrated the presence of the intended stacking sequences, extensive rotational disorder and atomically abrupt interfaces between the constituent layers. All compounds exhibit metallic character for temperature dependent resistivity. The carrier concentration varies systematically with the thickness of the thickest SnSe block in the isomer. Thicker blocks transfer more charge to the $NbSe_2$ units leading to fewer conducting holes. The mobility of the isomers decreases as the thickness of the $NbSe_2$ blocks decreases, indicating that there is more scattering in isolated $NbSe_2$ layers than in thicker slabs. The electrical properties suggest that the different structural constituents have separate functions, with SnSe acting as an electron donor to the conducting $NbSe_2$ layers. SnSe thickness controls the carrier concentration and the $NbSe_2$ thickness governs the carrier mobility. This suggests that such heterostructures can be tailored through choice of constituent, layer thicknesses and layer sequences to tune particular properties and enhance performance. A simple model was used to calculate properties from building blocks, but a theoretical model is needed to predict the optimal compound for specific properties

among the many potential compounds that can be prepared. The modest success of the simple model highlights how the properties within a family of compounds containing the same constituents are interrelated. This suggests that a theoretical model with parameters such as van der Waals bonding interactions and strong electron−electron correlation scaled to experimental data on a small number of compounds might be very successful in predicting properties of yet to be prepared compounds.

METHODS

The inorganic isomers were synthesized through the modulated elemental reactants (MER) technique,[28] which utilizes a custom-built vacuum chamber with a base pressure of 1×10^{-8} Torr. Three kW Thermionic electron beam guns were used to evaporate elemental sources of Sn (99.9% purity) and Nb (99.9% purity) at the rate of 0.04 and 0.02 nm/s, respectively, while a Knudsen effusion cell was used to deposit Se (99.9% purity) at a rate of 0.05 nm/s. INFICON Xtal microbalance quartz-crystal monitors placed 25 cm away from the elemental sources were used to monitor the rate of deposition. The precursors were deposited onto polished (100) oriented silicon wafers. A sequential LabView program and pneumatic shutters were used to control the deposition order and amount of material deposited, respectively. A detailed description of the synthesis technique is given elsewhere.[29,30] The precursors were annealed in an N_2 glovebox with O_2 < 0.6 ppm on a hot plate.

The film thickness and crystallinity were determined by X-ray reflectivity and diffraction measurements, respectively. High angle and low angle X-ray measurements were conducted on a Bruker AXS D8 diffractometer equipped with Göbel mirror and Bragg−Brentano optics geometry and a Cu Kα (0.154 nm) radiation source operated at 40 kV and 40 mA. In-plane X-ray data were obtained at the Advanced Photon Source (APS) at the Argonne National Laboratories, Beamline-33-C with an incident X-ray wavelength of 0.1265 nm. Peak positions and intensities were evaluated using standard peak shape functions. The intensities were obtained by integration of the peak areas. The in-plane crystallite size for $NbSe_2$ was calculated applying the Scherrer equation to the only nonoverlapping independent $NbSe_2$ reflections, (110) and (120). We assumed that all of the decreased coherence length of the scattering results from crystallite size, which permits a qualitative comparison of the in plane scattering differences between the six compounds. Atomic composition of the isomers was determined on a Cameca SX-100 electron probe microanalyzer (EPMA) equipped with five wavelength dispersive spectrometers using a thin film technique developed by Donovan *et al.*[31]

High angle annular dark field-scanning transmission electron microscopy (HAADF-STEM) samples were prepared using an FEI Helios Nanolab 600 Dual Beam focused ion beam (FIB) with methods modified from Schaffer *et al.*[32] and were imaged using an FEI Titan 80−300.

Electrical transport measurements were conducted on a custom-built instrument using a standard van der Pauw technique. Samples for transport measurements were deposited onto fused quartz silica in a van der Pauw geometry. Contacts were made to the four corners of the cross using indium. Current was injected through two of the cross arms, and the potential drop between the remaining cross arms was measured using a Keithley 2181A nanovoltmeter. From the current−potential plot, the sheet resistance of the film was obtained. With the use of total film thickness, the sheet resistance was converted to resistivity. Temperature dependent measurements were conducted between 10 and 295 K using a helium cryostat. Hall effect measurements were conducted by varying the magnetic field using an electromagnet at a constant current of 0.100 mA. The slope of the Hall voltage *vs* magnetic field was used to determine the Hall coefficient, which in turn was used to determine carrier concentration assuming a single band model.

Conflict of Interest: The authors declare no competing financial interest.

Acknowledgment. The authors thank R. Fischer and J. Razink from CAMCOR for assistance in preparing TEM samples and collecting STEM images. Grant MRI 0923577 provided funding for the dual beam FIB used to make TEM cross sections. The authors acknowledge support from the National Science Foundation under grant DMR-1266217. Co-author M. Falmbigl acknowledges support from the National Science Foundation through CCI grant number CHE-1102637. The authors thank J. Karapetrova for assistance at Beamline 33-C at the Advanced Photon Source (APS) in Argonne National Laboratories. The use of the APS was supported by the U.S. Department of Energy, Office of Science, and the Office of Basic Energy Sciences, under Contract No. DE-AC02-06CH11357.

Supporting Information Available: Additional HAADF-STEM images showing larger areas of the compounds 4:**4** and 2:**1**:1:**2**:1:**1**. This material is available free of charge *via* the Internet at http://pubs.acs.org.

REFERENCES AND NOTES

1. *Handbook of Nanotechnology*, 3rd ed.; Bhushan, B., Ed.; Springer: Berlin Heidelberg, 2010; p 1964.
2. Minnich, A. J.; Dresselhaus, M. S.; Ren, Z. F.; Chen, G. Bulk Nanostructured Thermoelectric Materials: Current Research and Future Prospects. *Energy Environ. Sci.* **2009**, *2*, 466.
3. Zhao, L.-D.; Lo, S.-H.; Zhang, Y.; Sun, H.; Tan, G.; Uher, C.; Wolverton, C.; Dravid, V. P.; Kanatzidis, M. G. Ultralow Thermal Conductivity and High Thermoelectric Figure of Merit in SnSe Crystals. *Nature* **2014**, *508*, 373–377.
4. Shakouri, A. Recent Developments in Semiconductor Thermoelectric Physics and Materials. *Annu. Rev. Mater. Res.* **2011**, *41*, 399–431.
5. Dresselhaus, M. S.; Chen, G.; Tang, M. Y.; Yang, R. G.; Lee, H.; Wang, D. Z.; Ren, Z. F.; Fleurial, J.-P.; Gogna, P. New Directions for Low-Dimensional Thermoelectric Materials. *Adv. Mater.* **2007**, *19*, 1043–1053.
6. Liu, G.; Ji, S.; Xu, G.; Ye, C. Interface Engineering: Boosting the Energy Conversion Efficiencies for Nanostructured Solar Cells. *Pure Appl. Chem.* **2012**, *84*, 2653–2675.
7. Ma, C.; Liu, M.; Liu, J.; Collins, G. Interface Effects on the Electronic Transport Properties in Highly Epitaxial $LaBaCo_2O_5$ Films. *ACS Appl. Mater. Interfaces* **2014**, 6–11.
8. Noh, M.; Johnson, C. D.; Hornbostel, M. D.; Thiel, J.; Johnson, D. C. Control of Reaction Pathway and the Nanostructure of Final Products through the Design of Modulated Elemental Reactants. *Chem. Mater.* **1996**, *8*, 1625–1635.
9. Beekman, M.; Heideman, C. L.; Johnson, D. C. Ferecrystals: Non-Epitaxial Layered Intergrowths. *Semicond. Sci. Technol.* **2014**, *29*, 064012.
10. Heideman, C.; Tepfer, S.; Lin, Q.; Rostek, R.; Zschack, P.; Anderson, M. D.; Anderson, I. M.; Johnson, D. C. Designed Synthesis, Structure, and Properties of a Family of Ferecrystalline Compounds $[(PbSe)_{1.00}]_m(MoSe_2)_n$. *J. Am. Chem. Soc.* **2013**, *135*, 11055–11062.
11. Moore, D. B.; Beekman, M.; Disch, S.; Johnson, D. C. Telluride Misfit Layer Compounds: $[(PbTe)_{1.17}]_m(TiTe_2)_n$. *Angew. Chem., Int. Ed.* **2014**, *53*, 5672–5675.
12. Alemayehu, M. B.; Falmbigl, M.; Ta, K.; Grosse, C.; Westover, R. D.; Bauers, S. R.; Fischer, S. F.; Johnson, D. C. Structural and Electrical Properties of $([SnSe]_{1+\delta})_m(NbSe_2)_1$ Compounds: Single $NbSe_2$ Layers Separated by Increasing Thickness of SnSe. *Chem. Mater.* **2015**, *27* (3), 867–875.

13. Esters, M.; Alemayehu, M. B.; Jones, Z.; Nguyen, N. T.; Anderson, M. D.; Grosse, C.; Fischer, S. F.; Johnson, D. C. Inorganic Structural Isomers Synthesized By Diffusion Constrained Self-Assembly of Designed Precursors—A Novel Type of Isomerism. *Angew. Chem., Int. Ed.* **2015**, *54*, 1130–1134.
14. Alemayehu, M. B.; Falmbigl, M.; Grosse, C.; Ta, K.; Fischer, S. F.; Johnson, D. C. Structure and Electrical Properties of a New $([SnSe]_{1.16})_1(NbSe_2)_1$ Polytype. *J. Alloys Compd.* **2015**, *619*, 861–868.
15. Atkins, R.; Wilson, J.; Zschack, P.; Grosse, C.; Neumann, W.; Johnson, D. C. Synthesis of $[(SnSe)_{1.15}]_m(TaSe_2)_n$ Ferecrystals: Structurally Tunable Metallic Compounds. *Chem. Mater.* **2012**, *24*, 4594–4599.
16. Atkins, R.; Disch, S.; Jones, Z.; Haeusler, I.; Grosse, C.; Fischer, S. F.; Neumann, W.; Zschack, P.; Johnson, D. C. Synthesis, Structure and Electrical Properties of a New Tin Vanadium Selenide. *J. Solid State Chem.* **2013**, *202*, 128–133.
17. Beekman, M.; Disch, S.; Rouvimov, S.; Kasinathan, D.; Koepernik, K.; Rosner, H.; Zschack, P.; Neumann, W. S.; Johnson, D. C. Controlling Size-Induced Phase Transformations Using Chemically Designed Nanolaminates. *Angew. Chem., Int. Ed.* **2013**, *52*, 13211–13214.
18. Falmbigl, M.; Fiedler, A.; Atkins, R. E.; Fischer, S. F.; Johnson, D. C. Suppressing a Charge Density Wave by Changing Dimensionality in the Ferecrystalline Compounds $([SnSe]_{1.15})_1(VSe_2)_n$ with n = 1, 2, 3, 4. *Nano Lett.* **2015**, *15* (2), 943–948.
19. Alemayehu, M. B.; Falmbigl, M.; Ta, K.; Johnson, D. C. Effect of Local Structure of $NbSe_2$ on the Transport Properties of $[(SnSe)_{1.16}]_1[(NbSe_2)]_n$ Ferecrystals. *Chem. Mater.* **2015**, *27* (6), 2158–2164.
20. Kadijk, F. Niobium and Tantalum Diselenides. *Recl. Trav. Chim. Pays-Bas* **1964**, *83*, 768–775.
21. Kadijk, F. On The Polymorphism Of Niobium Diselenide. *J. Less Common Met.* **1971**, *23*, 437–441.
22. Atkins, R.; Moore, D. B.; Johnson, D. C. Insights into the Self-Assembly of Ferecrystalline Compounds from Designed Amorphous Precursors. *Chem. Mater.* **2013**, *25*, 1744–1750.
23. Moore, D.; Beekman, M.; Disch, S.; Zschack, P.; Häusler, I.; Neumann, W.; Johnson, D. C. Synthesis, Structure, and Properties of Turbostratically Disordered $(PbSe)_{1.18}(TiSe_2)_2$. *Chem. Mater.* **2013**, *25*, 2404–2409.
24. Lee, H. N. S. The Low-Temperature Transport Properties of $NbSe_2$. *J. Appl. Phys.* **1969**, *40*, 602.
25. Alemayehu, M. B.; Ta, K.; Falmbigl, M.; Johnson, D. C. Structure, Stability and Properties of the Intergrowth Compounds $([SnSe]_{1+\delta})_m(NbSe_2)_1$, where $m = n = 1-20$. *J. Am. Chem. Soc.* **2015**, 10.1021/jacs.5b01556.
26. Wiegers, G. A. Misfit Layer Compounds: Structures and Physcial Properties. *Prog. Solid State Chem.* **1996**, *24*, 1–139.
27. Alemayehu, M. B.; Ta, K.; Falmbigl, M.; Johnson, D. C. Charge Transfer vs. Dimensionality: What Affects the Transport Properties of Ferecrystals? *Nanoscale* **2015**, 10.1039/c4nr07338j.
28. Fister, L.; Johnson, D. C. Controlling Solid-State Reaction Mechanisms Using Diffusion Length Ultrathin-Film Superlattice Composite. *J. Am. Chem. Soc.* **1992**, *114*, 4639–4644.
29. Lin, Q.; Smeller, M.; Heideman, C. L.; Zschack, P.; Koyano, M.; Anderson, M. D.; Kykyneshi, R.; Keszler, D. A.; Anderson, I. M.; Johnson, D. C. Rational Synthesis And Characterization Of A New Family Of Low Thermal Conductivity Misfit Layer Compounds $[(PbSe)_{0.99}]_m(WSe_2)_n$. *Chem. Mater.* **2010**, *22*, 1002–1009.
30. Noh, M.; Thiel, J.; Johnson, D. C. Synthesis of Crystalline Superlattices by Controlled Crystallization of Modulated Reactants. *Adv. Sci.* **1995**, *270*, 1181–1184.
31. Donovan, J. J.; Tingle, T. N. An Improved Mean Atomic Number Background Correction for Quantitative Microanalysis. *Microsc. Soc. Am.* **1996**, *2*, 1–7.
32. Schaffer, S.; Schaffer, B.; Ramasse, Q. Sample Preparation for Atomic Resolution STEM at Low Voltages by FIB. *Ultramicroscopy* **2012**, *114*, 62–71.